

Cite this: DOI: 10.1039/c0xx00000x

www.rsc.org/xxxxxx

ARTICLE TYPE

New hybrid materials with porphyrin-ferrocene and porphyrin-pyrene covalently linked to single-walled carbon nanotubes.

Solon P. Economopoulos,^a Angeliki Skondra,^b Kalliopi Ladomenou,^b Nikolaos Karousis,^a Georgios Charalambidis,^b Athanassios G. Coutsolelos^{*b} and Nikos Tagmatarchis^{*a}

⁵ Received (in XXX, XXX) Xth XXXXXXXXXX 20XX, Accepted Xth XXXXXXXXXX 20XX

DOI: 10.1039/b000000x

Novel porphyrin derivatives bearing additional pyrene or ferrocene units as light harvesting antenna systems were synthesized and fully characterized. Following a covalent functionalization approach for single-walled carbon nanotubes (SWCNTs), stable SWCNT suspensions in common organic solvents were produced. Subsequently, the resulting porphyrin-pyrene and porphyrin-ferrocene dyads were incorporated onto the nanotubes' backbone yielding donor-donor-acceptor hybrids. The resulting hybrid materials were soluble in common organic solvents and were characterized using micro-Raman, ATR-IR, UV-Vis and photoluminescence spectroscopy, transmission electron microscopy, thermogravimetric analysis and electrochemistry. Photoluminescence quenching of the porphyrin emission in both hybrid materials was detected thus suggesting the potentiality of these materials in photoelectrochemical cells.

1. Introduction

The last couple of decades a new interdisciplinary area in material science and applications has emerged. Various unique structures of nanomaterials, such as fullerenes, carbon nanotubes (CNTs) and graphene, possess remarkable mechanical, thermal, and optical properties making them suitable for an array of technological applications in electronics, advanced materials, and nanomedicine. Their inherent desirable properties are only enriched through the process of chemical modification and improving upon solubility and processability, but also offering the opportunity to tune the physical properties

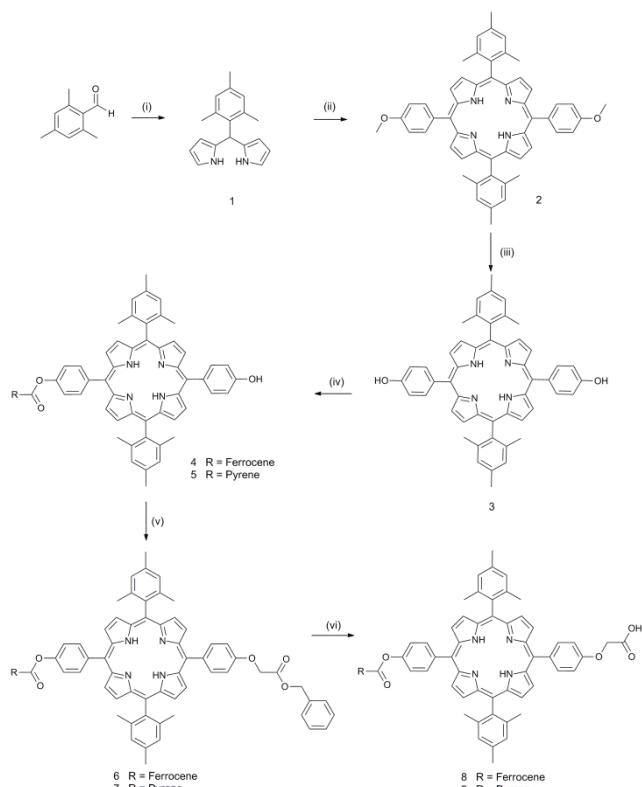
Single wall carbon nanotubes (SWCNTs) exhibit interesting electronic properties¹ rivalling the ones of buckminsterfullerene, while maintaining excellent mechanical properties. Furthermore, SWCNTs exhibit very high tensile strength and excellent thermal and electrical conductivity, while their high aspect ratio and nanoscale size make them a great candidate in diverse nanotechnology applications.² The main drawback of CNTs, that is the poor solubility properties, is countered by chemical functionalization. Therefore, synthetic efforts have focused on the functionalization of SWCNTs³ thus affording materials soluble in common organic solvents. Solubilizing CNTs will permit their easier incorporation in organic electronic devices with low-cost widespread processing techniques. Modern synthetic efforts have focused on coupling moieties with electro- or photo-active properties onto SWCNTs affording donor acceptor architectures with interesting optoelectronic properties.^{4,5} This motif has also been realized for carbon nanohorns (CNHs)^{6,7} and lately graphene sheets.^{8,9}

The idea of adding a second light harvesting moiety to the solar cell active layer is not novel and several synthetic efforts have been made towards the realization of this concept in

fullerenes giving rise to triads.^{10,11} Careful design or selection of the chromophore(s) to include multiple photon absorbers in a single system is an intriguing approach that opens up new pathways towards developing an efficient solar absorber extending to the near-IR region.¹² On the other hand as a standalone active moiety the realization of donor-acceptor-donor architectures can prove extremely efficient in various fields ranging from sensors¹³ to optoelectronics.¹⁴⁻¹⁷

Porphyrins, being the basis for chlorophyll, the natural photon absorbing moiety of the plants, are an excellent candidate for organic solar cells, providing light harvesting properties as well as being bulky molecules that can aid in solubilization. Fullerene-porphyrin structures have been studied extensively as they provide a stable platform for studying the properties of donor-acceptor hybrids.¹⁸ The resulting molecule can act as a stand-alone active system providing electron donating properties, owed to the porphyrin moiety and electron accepting properties, due to the carbon nanostructure. This has been attempted preliminary on a non-covalent basis,¹⁹ but there are also many examples of porphyrin-SWCNT nanohybrids linked with covalent bonding.^{5,20,21} The addition of a second light-harvesting moiety that acts synergistically with the porphyrin will give rise to donor-donor-acceptor structures. In an example of this type of structures the electron donor ferrocene (Fc) was used in porphyrin and fullerene systems to construct multicomponent systems.²² In a very recent example a covalent linked Fc-porphyrin-SWCNT hybrid material has been synthesized via amidation reaction between an oxidized SWCNTs and an amino-terminated porphyrin moiety carrying a Fc unit.²³

Herein, we present the covalent conjugation of porphyrin-ferrocene and porphyrin-pyrene moieties onto pre-modified SWCNTs. The newly formed SWCNT-based hybrids were found



Scheme 1 Synthetic procedure for the preparation of porphyrin derivatives **8** and **9**. (i) pyrrole, TFA; (ii) 4-methoxybenzaldehyde, TFA, DDQ, CH₂Cl₂; (iii) BBr₃, CH₂Cl₂ then CH₃OH, H₂O; (iv) Et₃N, ferrocene-1-carbonyl chloride for **4** or pyrene-1-carbonyl chloride for **5**; (v) benzyl 2-bromoacetate, K₂CO₃, DMF; (vi) H₂, 10% Pd/C, THF.

soluble in common organic solvents and fully characterized with complementary spectroscopic, thermal and microscopy techniques, while their photochemical and electrochemical properties were also evaluated.

2. Experimental

2.1. Synthesis of 5-(4-(carboxymethoxy)phenyl)-15-(4-(ferrocene-2-carboxyloxy)phenyl)-10,20-bis(2,4,6-trimethylphenyl)porphyrin **8**.

A solution of porphyrin **6** (15 mg, 0.01 mmol) and 10 % Pd/C (5 mg, 0.05 mmol) in THF (5 mL) was stirred under H₂ at room temperature overnight. Then the mixture was filtered on a pad of celite and the solid washed first with THF (5 mL) and then with MeOH (5 mL). The solvents were removed from the filtrate and the resulting solid was purified by column chromatography (1–20 % methanol in dichloromethane). The desired product was obtained using 20 % MeOH in CH₂Cl₂ to give **8** as a purple solid (9.5 mg, 95 %). ¹H NMR (500 MHz, CDCl₃): δ 8.87 (d br, 2H), 8.80 (d br, 2H), 8.71 (m, 4 H), 8.27 (d, *J* = 6.0 Hz, 2H), 8.16 (d, *J* = 5.0 Hz, 2H), 7.59 (d, *J* = 7.5 Hz, 2H), 7.29 (s br, 6H, H₃), 5.1 (s, 2H), 4.92 (s br, 2H), 4.60 (s, 2H), 4.43 (s, 5H), 2.63 (s, 6H), 1.85 (s, 12H), -2.65 (s, 2H); ¹³C NMR (75 MHz, CDCl₃): δ 171.6, 170.6, 157.3, 150.8, 139.4, 138.4, 137.8, 135.7, 135.4, 131.5, 130.2, 127.8, 120.1, 118.4, 113.0, 72.1, 70.8, 70.1, 65.2, 21.6, 21.5; UV/vis (CH₂Cl₂) λ_{max}, nm (ε, mM⁻¹ cm⁻¹) 419 (441.2), 447 (23.1), 515 (16.9), 550 (6.7), 591 (4.8), 647 (3.7); HRMS (MALDI-TOF) calcd for C₆₃H₅₃FeN₄O₅ [M+H]⁺ 1001.3365,

found 1001.3372.

2.2. Synthesis of 5-(4-(carboxymethoxy)phenyl)-15-(4-(pyrene-1-carboxyloxy)phenyl)-10,20-bis(2,4,6-trimethylphenyl)porphyrin **9**.

A solution of porphyrin **7** (25 mg, 0.02 mmol) and 10 % Pd/C (8 mg, 0.08 mmol) in THF (5 mL) was stirred under H₂ at room temperature overnight. Then the mixture was filtered on a pad of celite and the solid washed first with THF (5 mL) and then with MeOH (5 mL). The solvents were removed from the filtrate and the resulting solid was purified by column chromatography (CH₂Cl₂/MeOH 7:3). The desired product was obtained using CH₂Cl₂/MeOH 7:3 to give **9** as a purple solid (19 mg, 93 %). ¹H NMR (300 MHz, CDCl₃): δ 9.57 (m, 1H), 9.10 (m, 1H), 8.92 (d br, 2H), 8.80 (d br, 2H), 8.73 (m, 4H), 8.37–8.14 (m, 11H), 7.78 (d, *J* = 7.8 Hz, 2H), 7.30 (s, 4H), 7.26 (s br, 2H), 2.64 (s, 6H), 1.87 (s, 12H), -2.55 (s, 2H); ¹³C NMR (75 MHz, CDCl₃): δ 171.2, 166.5, 157.4, 151.2, 140.4, 139.5, 138.4, 137.9, 135.6, 135.2, 132.2, 131.1, 130.4, 130.3, 129.2, 128.5, 127.9, 127.3, 126.6, 125.1, 124.9, 124.3, 122.0, 120.3, 118.7, 114.4, 113.1, 65.1, 21.7, 21.5; UV/vis (CH₂Cl₂) λ_{max}, nm (ε, mM⁻¹ cm⁻¹) 284 (31.5), 357 (32.0), 419 (349.3), 515 (15.8), 550 (6.9), 591 (5.1), 647 (3.9); HRMS (MALDI-TOF) calcd for C₆₉H₅₃N₄O₅ [M+H]⁺ 1017.4016, found 1017.4022.

2.3. Synthesis of hybrid materials **11** and **12**.

A solution of ferrocene-porphyrin **8** or pyrene-porphyrin **9**, 1-(3-dimethylaminopropyl)-3-ethylcarbodiimide hydrochloride (5 equiv.) and 1-hydroxy-benzotriazole (5 equiv.) in chloroform (10 mL) was stirred for 30 min. at room temperature and then was added to a triethylamine-neutralized solution of ammonium-functionalized SWCNTs **10**²⁴ (20 mg) in chloroform (15 mL). The reaction mixture was stirred at room temperature for 48 h and then was filtered through PTFE membrane filter (pore size 0.2 μm) and washed with dichloromethane (100 mL), methanol (100 mL) and diethylether (50 mL).

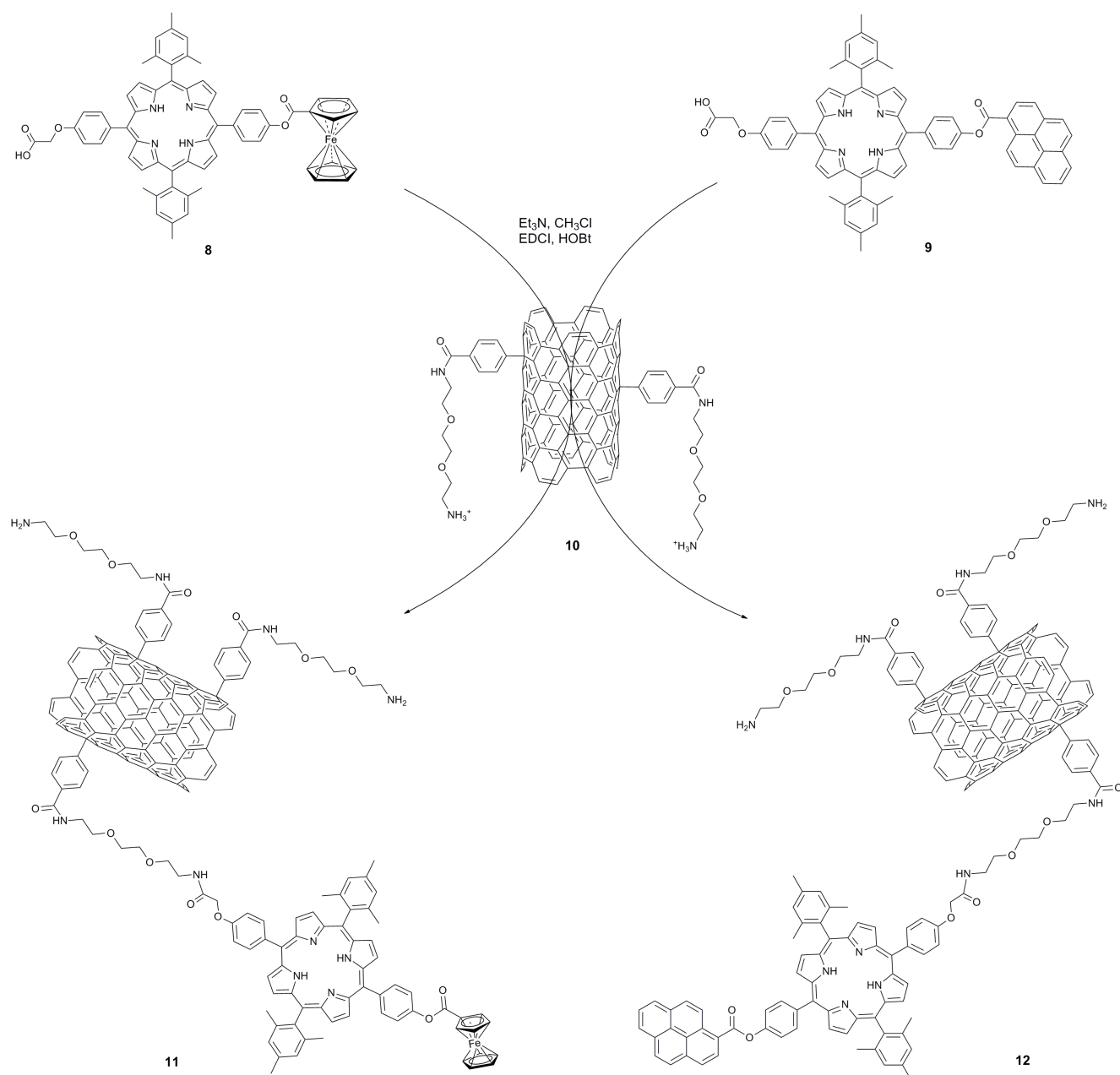
3. Results and Discussion

The synthesis of ferrocene-porphyrin **8** and pyrene-porphyrin **9** – abbreviated as H₂P-Fc and H₂P-pyr, respectively – is schematically shown in Scheme 1. Briefly, acid-catalyzed reaction of 4-methoxybenzaldehyde and 2,2'-(2,4,6-trimethylphenyl)methylenebis(1H-pyrrole) **1**, followed by demethylation in the presence of boron tribromide, afforded 5,15-bis(4-hydroxyphenyl)-10,20-bis(2,4,6-trimethylphenyl)porphyrin **3**. At this point it is important to note that the sterically demanding 2,4,6-trimethylphenyl moiety present as a substituent of the bis(1H-pyrrole)methane was deliberately chosen due to its ability to afford trans-meso substituted porphyrins without scrambling, thus avoiding the formation of a complicated mixture of porphyrins. Then, selective condensation reaction of porphyrin **3** with either ferrocene or pyrene carbonyl chloride yielded mono-substituted porphyrins **4** and **5**, respectively, possessing a free hydroxyl group at the meso-position. The latter was subsequently coupled with benzyl bromo acetate to result protected analogues **6** and **7**. Successful cleavage of the benzyl group after catalytic hydrogenation afforded the final porphyrin products bearing ferrocene for **8** and pyrene groups for **9**,

Cite this: DOI: 10.1039/c0xx00000x

www.rsc.org/xxxxxx

ARTICLE TYPE



Scheme 2 Synthetic procedure for the preparation of the SWCNT-(H₂P-Fc) **11** and SWCNT-(H₂P-pyr) hybrid materials **12**

respectively. The structure of all synthesized compounds was verified by ¹H and ¹³C NMR spectroscopy as well as MALDI TOF mass spectrometry (Figs. S1-S16 in ESI†).

In a parallel route, SWCNTs were functionalized by the widely applied methodology of in-situ generated aryl diazonium salts addition.²⁵ In this context, aryl units possessing at para-position a polar ethylene glycol chain terminating with a Boc amino-protected group were successfully introduced onto the skeleton of SWCNTs. Then, under acidic conditions, the free amino-units

were liberated and porphyrin derivatives **8** and **9** were covalently attached to the amino-modified SWCNTs **10**, by a typical condensation reaction, according to Scheme 2. The hybrid materials **11** and **12** form stable dispersions in a range of polar solvents like dichloromethane, methanol and *N,N*-dimethylformamide, thus allowing their spectroscopic characterization and to perform studies of their properties in solution.

The morphological characterization of SWCNT-(H₂P-Fc) **11**

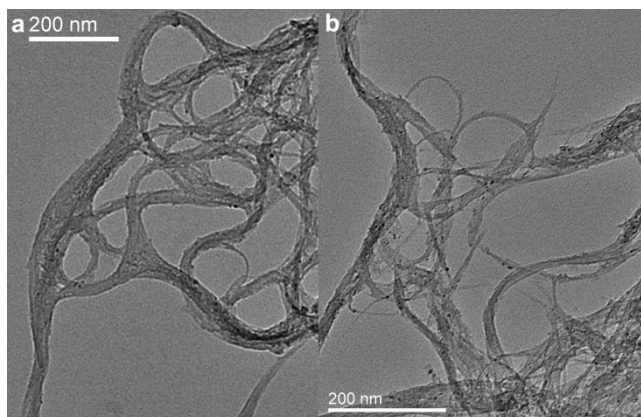


Fig. 1 Representative TEM images of a) SWCNT-(H₂P-Fc) **11** and b) SWCNT-(H₂P-pyr) **12** hybrid materials.

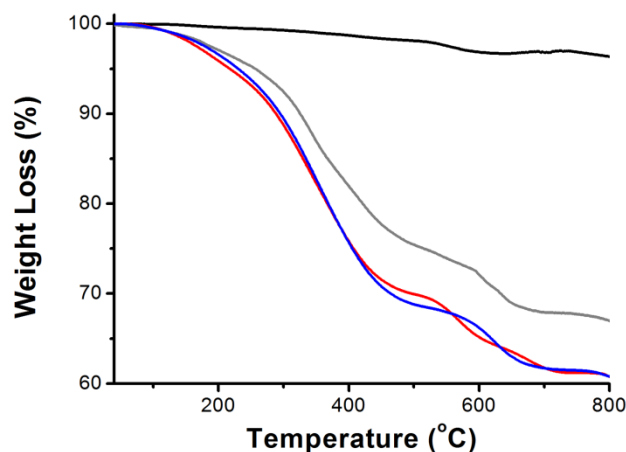


Fig. 2 TGA graphs of pristine SWCNTs (black), ammonium-functionalized SWCNTs **10** (gray), SWCNT-(H₂P-Fc) **11** (red) and SWCNT-(H₂P-pyr) **12** (blue), obtained under nitrogen.

and SWCNT-(H₂P-pyr) **12** was achieved by transmission electron microscopy (TEM). Representative TEM images (Fig. 1) of **11** and **12** reveal the presence of small bundles (10-90 nm in diameter) of SWCNTs. Moreover, no significant damage of the SWCNT backbone skeleton due to the functionalization is observed.

Spectroscopic insight on the formation of SWCNT-(H₂P-Fc) **11** and SWCNT-(H₂P-pyr) **12** hybrid materials was delivered by vibrational spectroscopy. Attenuated-total-reflectance infra-red (ATR-IR) spectroscopy indicates the C=O stretching vibrations due to carbonyl amides at 1640 cm⁻¹ and carboxylic esters at 1720 cm⁻¹, while the C-H stretching vibrations at 2843 and 2922 cm⁻¹ are also observed (Fig. S17 in ESI†).

Raman spectroscopy provided efficient support for the successful covalent functionalization of SWCNTs. Basically the Raman spectrum of aryl functionalized SWCNTs **10** exhibits two bands at 1336 and 1591 cm⁻¹. The former, D-band, is assigned to sp³-bonded carbon atoms and the latter, G-band, to sp² ones. For the aryl-functionalized SWCNT material the Raman spectrum shows an increased D-band (Fig. S18 in ESI†), while the I_D/I_G ratio found enhanced as compared with that for intact SWCNTs (I_D/I_G = 0.28 vs I_D/I_G = 0.12). Thus, that observation reflects the presence of sp³-hybridized carbons due to the attachment of the aryl moieties onto SWCNTs. However, the conjugation of porphyrin moieties, in the form of H₂P-Fc **8** and H₂P-pyr **9**, onto the already modified SWCNTs **10** does not significantly change the nature of the Raman spectrum (Fig. S19 in ESI†), as no further disruption on the carbon skeleton of SWCNTs occurs.

Thermogravimetric analysis (TGA) is a powerful tool to determine the degree of functionalization. Pristine SWCNTs are thermally intact and stable up to at least 800 °C under nitrogen atmosphere. Ammonium-functionalized SWCNTs **10** show a weight loss of 24 %, occurring in the temperature range of 200–580 °C, attributed to the decomposition of the aryl units grafted onto the surface of the nanotubes (Fig. 2). Taking into account the above value, the degree of functionalization was calculated and found to be 1 aryl ethylene glycol side chain per 73 carbon atoms of SWCNT material. TGA analysis for H₂P-Fc functionalized SWCNTs **11** and H₂P-pyr functionalized SWCNTs **12**, performed under same conditions, showed a weight loss of 27% and 30%, respectively, up to 550 °C, corresponding to the decomposition of the total organic matter grafted onto the surface

of the nanotubes framework. Based on that, it is evaluated that 1 H₂P-Fc based organic moiety for every 267 carbon atoms is present onto the functionalized SWCNTs **11** and 1 H₂P-pyr based organic moiety for every 239 carbon atoms for hybrid material **12**. By simply correlating those values with the one mentioned above for the ammonium-functionalized SWCNTs **10**, it is understood that approximately only one out of four -NH₂ units were condensed with the appropriate H₂P-Fc and H₂P-pyr moiety. Nevertheless, the latter can be rationalized when considering steric hindrance phenomena introduced by the large volume modified porphyrins occupy onto the SWCNT surface. The weight loss above 600 °C is attributed to decomposition of miscellaneous forms of disordered carbon²⁶ and due to the defects introduced on the carbon backbone through the functionalization procedure.

Due to the long chain that can act as spacer, hybrid materials **11** and **12** can provide interesting optical properties as recently demonstrated on graphene donor-spacer-acceptor hybrids.²⁷ As hybrid materials **11** and **12** show enhanced solubility in DMF and since optically active moieties have been attached to the SWCNTs' backbone, absorption and photoluminescence spectroscopy can be applied for evaluating the optical properties of the synthesized materials. In Fig. 3 the absorption spectra of SWCNT-(H₂P-Fc) **11** and SWCNT-(H₂P-pyr) **12** hybrid materials are compared with those ones derived from the unbound H₂P-Fc **8** and H₂P-pyr **9**. In the electronic absorption spectrum of **8** the predominant Soret band at 420 nm as well as the Q bands at 516, 551 and 594 and 650 nm are clearly observed (Fig. 3a). Hybrid material **11** shows a continuous absorption in the UV-Vis spectrum common for SWCNTs with a clear shoulder at 424 nm, corresponding to the Soret band, red-shifted by 4 nm as compared with that of unbound **8**. Similarly, the UV-Vis spectrum of H₂P-pyr **9** shows the characteristic Soret band at 419 nm as well as the Q bands at 515, 550, 592 and 648 nm, while in the corresponding UV-Vis spectrum of SWCNT-(H₂P-pyr) **12** a clear shoulder at 422 nm, corresponding to the Soret band, red-shifted by 2 nm as compared with that of unbound **9** is found (Fig. 3b). These observations are in line with both the success of the linkage of H₂P-Fc **8** and H₂P-pyr **9**, respectively, to aryl-modified SWCNTs **10** and more importantly

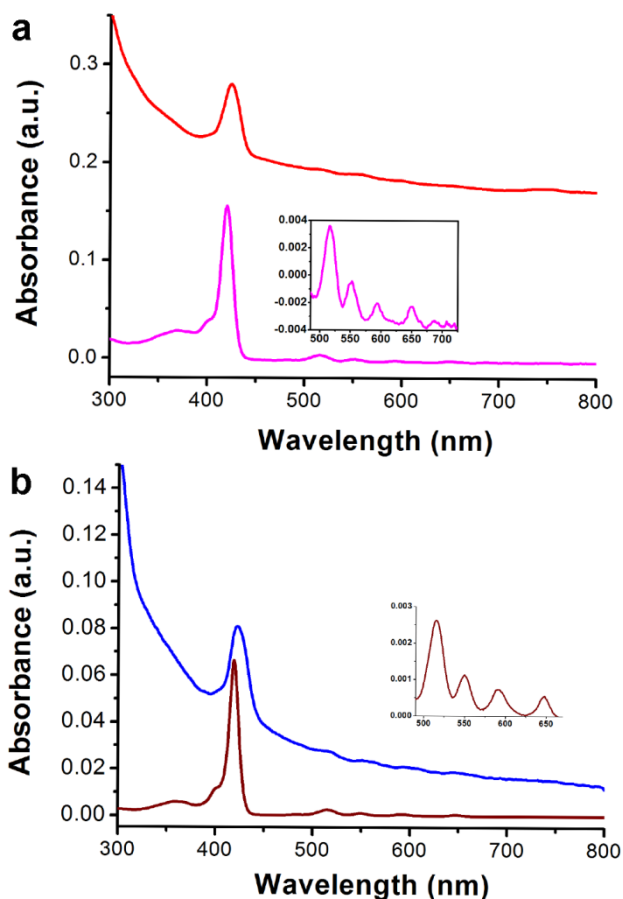


Fig. 3 UV-Vis absorption spectra of a) H₂P-Fc **8** (magenta) and SWCNT-(H₂P-Fc) **11** (red), and b) H₂P-pyr **9** (brown) and SWCNT-(H₂P-pyr) **12** (blue).

5 to ground state electronic interactions between SWCNTs and H₂P-Fc in the SWCNT-(H₂P-Fc) **11** and H₂P-pyr in the SWCNT-(H₂P-pyr) **12** hybrid materials, respectively. However, weak inter-porphyrin interactions, most likely between porphyrins located on the same nanotube, should be also
 10 considered and taken into account. Notably, such results are in agreement with earlier studies based on other hybrid materials composed of different porphyrins bonded to SWCNTs, CNHs and graphene.^{7,28,29}

Insight on the electronic interplay between H₂P-Fc **8** and H₂P-
 15 pyr **9**, respectively, and SWCNTs in the excited state of hybrids **11** and **12** is derived from photoluminescence studies. Upon excitation at 420 nm, the strong fluorescence emission of porphyrin **8** at 653 nm was significantly quenched by the presence of SWCNTs in the SWCNT-(H₂P-Fc) **11**, when
 20 measurements performed with matching absorption of H₂P-Fc at the excitation wavelength (Fig. 4a). The latter observation is indicative of electronic interactions between the singlet excited state of ¹(H₂P-Fc)* and SWCNTs, thus suggesting that photoilluminated H₂P-Fc can transport electrons to the electron
 25 accepting SWCNTs, in hybrid material **11**. A similar phenomenon was observed for SWCNT-(H₂P-pyr) hybrid material **12** (Fig. 4b), namely, quenching of the characteristic strong emission of H₂P-pyr at 653 nm, when excited at 420 nm.

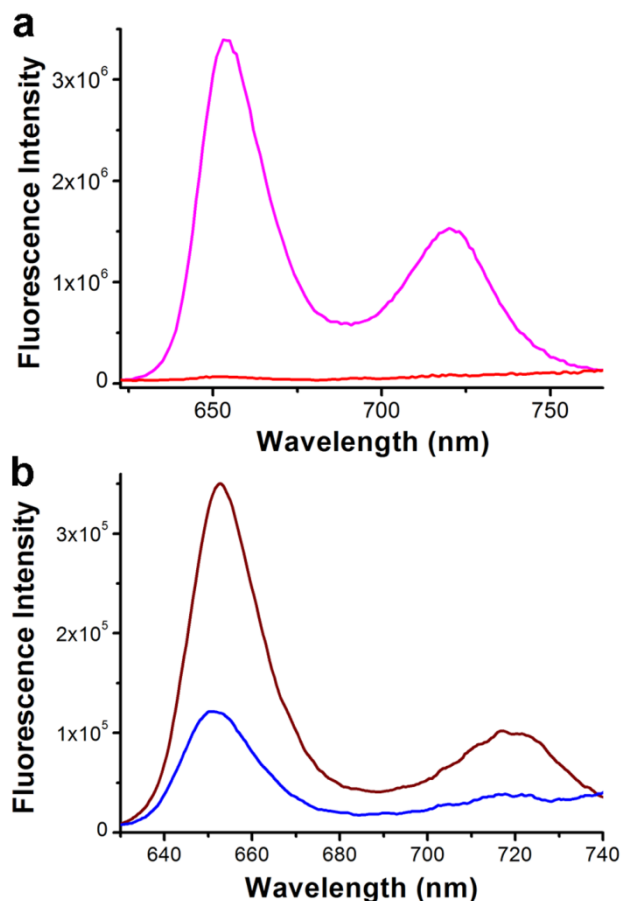


Fig. 4 Photoluminescence spectra of a) H₂P-Fc **8** (magenta) and SWCNT-(H₂P-Fc) **11** (red), and b) H₂P-pyr **9** (brown) and SWCNT-(H₂P-pyr) **12** (blue), upon excitation at 420 nm.

Finally, the energetics of the photoinduced process in SWCNT-(H₂P-Fc) **11** and SWCNT-(H₂P-pyr) **12** hybrid
 35 materials were evaluated by determining the corresponding redox potentials. Electrochemistry studies were performed by differential pulse voltammetry (DPV) in dry DMF, with [(*n*-Bu)₄NPF₆] as electrolyte. The materials were studied using a standard three electrode cell using Pt disc 1.6 mm diameter as a
 40 working electrode, Pt mesh as a counter electrode and Pt wire as a pseudo reference electrode. All voltammograms were calibrated vs Fc/Fc⁺. When examining H₂P-Fc **8** by DPV (reduction run), a clear one-electron reduction was observed at -1.62 V attributed to the porphyrin moiety as no appreciable signal from the ferrocene
 45 is expected at that potential (Fig. 5a). The same reduction peak slightly shifted by 50mV towards positive potentials was also observed in the SWCNT-(H₂P-Fc) hybrid material **11** along with a broad weak reduction at -0.50V attributed to the SWCNTs reduction.³⁰⁻³⁴ When scanning in positive potentials, **8** shows a
 50 reversible oxidation at 0.24V characteristic of the Fc moiety, and a very broad signal with peaks around 0.63 and 0.80V, owed to the presence of the porphyrin moiety. These three peaks are also present in the hybrid material **11**, but considerably lower in intensity. The peak assigned to the Fc moiety also has been
 55 shifted anodically by almost 180 mV denoting electronic interplay in the hybrid. The peaks assigned to the porphyrin moiety, remain unshifted in hybrid material **11**.

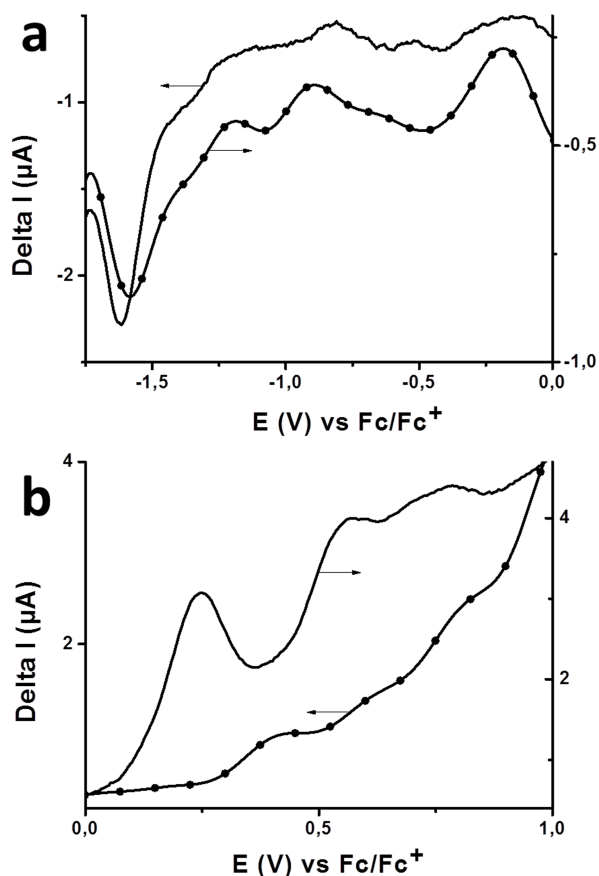


Fig. 5 Differential pulse voltammograms of H₂P-Fc **8** (solid line) and SWCNT-(H₂P-Fc) **11** (-●-), a) reduction, and b) oxidation runs.

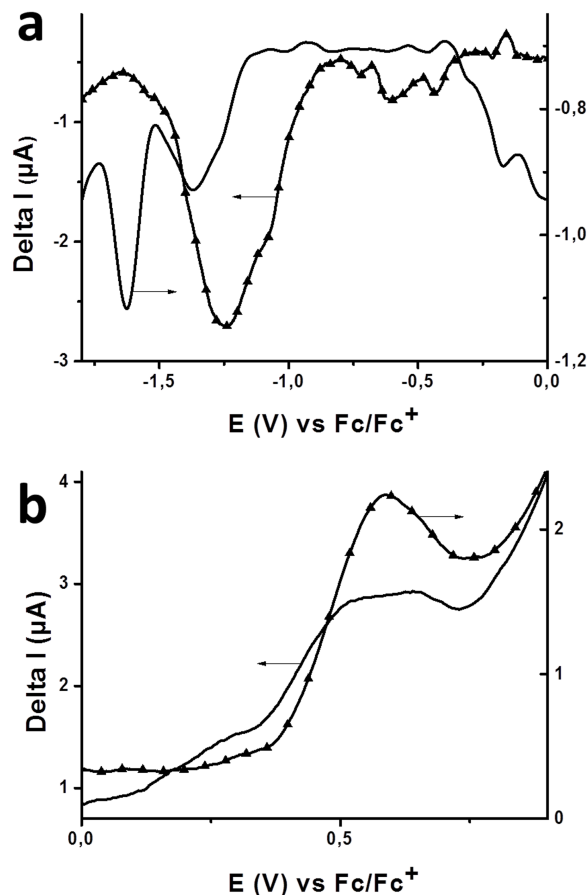


Fig. 6 Differential pulse voltammograms of H₂P-pyr **9** (solid line) and SWCNT-(H₂P-pyr) **12** (-▲-), a) reduction, and b) oxidation runs.

In Fig. 6 the DPV scans – reduction and oxidation runs – of materials **9** and **12** are presented. A pair of reduction processes takes place at negative potentials in **9** with peaks at -0.163 and -0.136 V. The former is a reduction also present in **8** so it is logical to assign this process to the reduction of the porphyrin moiety. The latter peak can be attributed to the pyrene moiety. When examining hybrid **12**, however, these processes are not observable but a rather strong signal at -1.25 V is present. This process, as was the case with hybrid **11**, is anodically shifted compared to **9**. A weak broad peak at -0.55V attributed to the SWCNTs reduction is also present in the DPV of **12**.³⁰⁻³⁴ In the oxidation run of the DPV a single process is present in both the dyad and the triad.

Table 1 Electrochemical data of the dyads and the triads synthesized.

Materials	E ^{ox} (V)	E _{HOMO} (eV)	E ^{red} (V)	E _{LUMO} (eV)	E _g ^{chem} (eV)
H ₂ P-Fc 8	0.24	5.34			
	0.63	5.73	-1.62	3.48	1.86
	0.80				
H ₂ P-pyr 9	0.57	5.67	-1.63	3.74	-1.93
			-1.36		
SWCNT-(H ₂ P-Fc) 11	0.42		-1.57		
	0.62		-0.50		
	0.81				
SWCNT-(H ₂ P-pyr) 12	0.59		-1.25		
			-0.55		

20

A very broad peak, centered at around 0.57 V is observed in the case of **9** and a basically unshifted peak at 0.59 but considerably lower in is observed in the case of hybrid **12**. Hence, the LUMO energy level of **9** is estimated at 3.74 eV, while the HOMO level is found at 5.67 eV. Collectively, all redox data are shown in Table 1.

3. Conclusions

Two SWCNT-based triads were synthesized and characterized. Porphyrin-ferrocene and porphyrin-pyrene functionalized SWCNTs hybrid materials **11** and **12** were fully characterized with the aid of complementary spectroscopic, thermal and microscopy techniques. The hybrid triads formed stable suspensions in common organic solvents. Photoluminescence measurements revealed the efficient quenching of the emission of photoexcited porphyrin in both SWCNT-(H₂P-Fc) **11** and SWCNT-(H₂P-pyrene) **12** hybrid materials suggesting that the individual components in the hybrid materials communicate each other via electron and/or energy transfer processes. The synthesized materials provide proof of concept for the incorporation of multiple chromophores onto the SWCNT backbone. The careful selection of light harvesting moieties absorbing throughout the visible spectrum and communicate electronically via covalent attachment to an acceptor moiety such as carbon nanotubes comprise a solid basis for highly efficient solar energy conversion devices.

Acknowledgments

N.T. acknowledges partial financial support from GSRT/ΕΣΠΑ 2007-2013 through actions “Postdoctoral support” project GRAPHCELL PE5(2126) and “ΣΥΝΕΡΓΑΣΙΑ” project 09ΣΥΝ-42-691-NANOKATAΛΥΣΗ as well as from COST network MP0901 NanoTP. A.G.C. acknowledges FP7-REGPOT-2008-1, project BIOSOLENUTI No 229927 from European Commission and Heraklitos grant from Ministry of Education of Greece and GSRT.

Notes and references

^a *Theoretical and Physical Chemistry Institute National Hellenic Research Foundation 48 Vassileos Constantinou Avenue, 11635 Athens, Hellas; Fax: + 30 210 7273794; Tel: + 30 210 7273835; E-mail: tagmatar@eie.gr*

^b *Department of Chemistry, University of Crete, P O Box 1470, 71409 Heraklion Crete, Hellas; Fax: + 30 2810 545161; Tel: + 30 2810 545045; E-mail: coutsole@chemistry.uoc.gr*

† Electronic Supplementary Information (ESI) available: [Experimental details; ¹H and ¹³C NMR, ATR-IR and Raman spectra]. See DOI: 10.1039/b000000x/

- 1 T. W. Odom, J.-L. Huang, P. Kim and C. M. Lieber, *Nature*, 1998, **391**, 62.
- 2 A. Vijayaraghavan, *J. Mater. Chem.*, 2012, **22**, 7083.
- 3 N. Karousis, N. Tagmatarchis and D. Tasis, *Chem. Rev.* 2010, **110**, 5366.
- 4 H. Murakami, T. Nomura and N. Nakashima, *Chem. Phys. Lett.*, 2003, **378**, 481.
- 5 Z. Guo, F. Du, D. Ren, Y. Chen, J. Zheng, Z. Liu and J. Tian, *J. Mater. Chem.*, 2006, **16**, 3021.
- 6 M. Vizuete, M. J. Gómez-Escalonilla, J. L. G. Fierro, A. S. D. Sandanayaka, T. Hasobe, M. Yudasaka, S. Iijima, O. Ito and F. Langa, *Chem.–Eur. J.*, 2010, **16**, 10752.
- 7 G. Pagona, G. E. Zervaki, A. S. D. Sandanayaka, O. Ito, G. Charalambidis, T. Hasobe, A. G. Coutsolelos and N. Tagmatarchis, *J. Phys. Chem. C*, 2012, **116**, 9439.
- 8 S. P. Economopoulos, G. Rotas, Y. Miyata, H. Shinohara and N. Tagmatarchis, *ACS Nano*, 2010, **4**, 7499.
- 9 T. Umeyama, J. Mihara, N. Tezuka, Y. Matano, K. Stranius, V. Chukharev, N. V. Tkachenko, H. Lemmetyinen, K. Noda, K. Matsushige, T. Shishido, Z. Liu, K. Hirose-Takai, K. Suenaga and H. Imahori, *Chem.–Eur. J.*, 2012, **18**, 4250.
- 10 F. D'Souza, M. E. El-Khouly, S. Gadde, M. E. Zandler, A. L. McCarty, Y. Araki and O. Ito, *Tetrahedron*, 2006, **62**, 1967.
- 11 Y. Matsuo, M. Maruyama, S. S. Gayathri, T. Uchida, D. M. Guldi, H. Kishida, A. Nakamura and E. Nakamura, *J. Am. Chem. Soc.*, 2009, **131**, 12643.
- 12 V. V. Diev, K. Hanson, J. D. Zimmerman, S. R. Forrest and M. E. Thompson, *Angew. Chem., Int. Ed.*, 2010, **49**, 5523.
- 13 M. Song, X. Wang, W. Liu and J. Zuo, *J. Colloid Interface Sci.*, 2010, **343**, 48.
- 14 E. Peeters, P. A. v. Hal, S. C. J. Meskers, R. A. J. Janssen and E. W. Meijer, *Chem.–Eur. J.*, 2002, **8**, 4470.
- 15 A. Gadisa, W. Mammo, L. M. Andersson, S. Admassie, F. Zhang, M. R. Andersson and O. Inganäs, *Adv. Funct. Mater.*, 2007, **17**, 3836.
- 16 M. P. O'Neil, M. P. Niemczyk, W. A. Svec, D. Gosztola, G. L. Gaines, III and M. R. Wasielewski, *Science*, 1992, **257**, 63.
- 17 S. J. K. Pond, M. Rumi, M. D. Levin, T. C. Parker, D. Beljonne, M. W. Day, J.-L. Bredas, S. R. Marder and J. W. Perry, *J. Phys. Chem. A*, 2002, **106**, 11470.
- 18 P. D. W. Boyd and C. A. Reed, *Acc. Chem. Res.*, 2005, **38**, 235.
- 19 F. D'Souza and O. Ito, *Chem. Commun.*, 2009, 4913.
- 20 S. Campidelli, C. Soambar, E. Lozano Diz, C. Ehli, D. M. Guldi and M. Prato, *J. Am. Chem. Soc.*, 2006, **128**, 12544.
- 21 T. Palacin, H. L. Khanh, B. Jousselme, P. Jegou, A. Filoramo, C. Ehli, D. M. Guldi and S. Campidelli, *J. Am. Chem. Soc.*, 2009, **131**, 15394.

- 22 H. Imahori, Y. Sekiguchi, Y. Kashiwagi, T. Sato, Y. Araki, O. Ito, H. Yamada and S. Fukuzumi, *Chem.–Eur. J.*, 2004, **10**, 3184.
- 23 H. Zhao, Y. Zhu, C. Chen, L. He and J. Zheng, *Carbon*, 2012, **50**, 4894.
- 24 N. Karousis, R. M. Papi, A. Siskos, P. Vakalopoulou, P. Glezakos, Y. Sarigiannis, G. Stavropoulos, D. A. Kyriakidis and N. Tagmatarchis, *Carbon*, 2009, **47**, 3550.
- 25 L. Bahr and J. M. Tour, *Chem. Mater.*, 2001, **13**, 3823.
- 26 H. N. Yehia, R. K. Draper, C. Mikoryak, E. K. Walker, P. Bajaj, I. H. Musselman, M. C. Daigrepont, G. R. Dieckmann and P. Pantano, *Journal of Nanobiotechnology*, 2007, **5**, 1.
- 27 A. Midya, V. Mamidala, J.-X. Yang, P. K. L. Ang, Z.-K. Chen, W. Ji and K. P. Loh, *Small*, 2010, **6**, 2292.
- 28 T. Umeyama, J. Mihara, H. Hayashi, N. Kadota, V. Chukharev, N. V. Tkachenko, H. Lemmetyinen, K. Yoshida, S. Isoda and H. Imahori, *Chem. Commun.*, 2011, **47**, 11781.
- 29 N. Karousis, A. S. D. Sandanayaka, T. Hasobe, S. P. Economopoulos, E. Sarantopoulou and N. Tagmatarchis, *J. Mater. Chem.*, 2011, **21**, 109.
- 30 D. Paolucci, M. M. Franco, M. Iurlo, M. Marcaccio, M. Prato, F. Zerbetto, A. Penicaud, and F. Paolucci, *J. Am. Chem. Soc.*, 2008, **130**, 7393.
- 31 Y. Tanaka, Y. Hirana, Y. Niidome, K. Kato, S. Saito, and N. Nakashima, *Angew. Chem. Int. Ed.*, 2009, **48**, 7655.
- 32 D. Ehli, C. Oelsner, D. M. Guldi, A. Mateo-Alonso, M. Prato, C. Schmidt, C. Backes, F. Hauke, and A. Hirsch, *Nat. Chem.*, 2009, **1**, 243.
- 33 A. S. D. Sandanayaka, E. Maligaspe, T. Hasobe, O. Ito, and F. D'Souza, *Chem. Commun.*, 2010, **46**, 8749.
- 34 F. D'Souza, S. K. Das, M. E. Zandler, A. S. D. Sandanayaka, and O. Ito, *J. Am. Chem. Soc.* 2011, **133**, 19922.